From Eq. 2, both core motion and the dissipative power at the CMB are inversely proportional to K_c at the time of resonance. For $K_c = 1.5 \times 10^{-7}$, there is a resonance amplification factor of about 10^4 with respect to the present value of the dissipative power: P_{CMB} may reach a few terawatts at the time of resonance; that is, it may have the same order of magnitude as the estimates for the present heat flux from the core to the mantle, which ranges from 10^{12} W to 9×10^{12} W (2). By time integration of the dissipative power, we compute the energy associated with a resonance event to be about 5×10^{25} J.

During times of resonance, the frictional power may be converted into heat (by ohmic heating and viscous friction) and destabilize the D″ thermal layer, leading to the generation of deep-mantle plumes. With a lag time between the time of resonance and the surface observations (16), these plumes may be responsible for continental flood basalt volcanism (such as the Siberian traps at 250 Ma) and may play a role in the formation of the continental crust in the Archaean or Proterozoic. The two major resonances between 4 Ga and 500 Ma occurred around 3 ± 0.2 Ga and 1.8 ± 0.2 Ga, for the 1/3-annual and semiannual tidal waves (shaded area in Fig. 1). These dates correspond to peaks in worldwide crustal production (Fig. 1B) (17, 18); thus, it seems possible to correlate the Precambrian resonance times with major crustforming episodes. The temperature near the ICB would increase during resonance periods. This effect could stop inner core growth (which may be responsible for the present dynamo processes) and lead to a new momentum equilibrium for the geodynamo. The temperature increase at the ICB may also enhance thermal convection within the fluid core, perturbing the fluid equilibrium.

One consequence of the core's dynamic seen at Earth's surface would be a change in the geomagnetic field, possibly changing the magnetic field reversal frequency. Consequently, we try to compare the times of major resonances with the geomagnetic field reversal frequency (19). Since 500 Ma, one correlation appears: The resonance of the annual solar tidal wave occurred at the end of the Kiamen Reverse Superchron (270 Ma) and may have restarted the reversal process. Simultaneously, this resonance destabilizes the D″ region, and 20 million years later, plumes arrived at Earth's surface from D″, producing widespread volcanism (Siberian traps) and mass extinction (Permo-Triassic limit).

References and Notes

1. P. Melchior, *Physique et Dynamique Planétaires, Géodynamique* (Vander, Brussels, 1973), vol. 4.
2. F. D. Stacey, *Physics of the Earth* (Brookfield, Brisbane, Australia, ed. 3, 1992).
3. H. Poincare, *Bull. Astron.* **27**, 321 (1910).
4. P. M. Mathews, B. A. Buffet, T. A. Herring, I. I. Shapiro, *J. Geophys. Res.* **96**, 8219 (1991).
5. V. Dehant, J. Hinderer, H. Legros, M. Lefftz, *Phys. Earth Planet. Inter.* **76**, 259 (1993).
6. A. Toomre, *Geophys. J. R. Astron. Soc.* **38**, 335 (1974).
7. J. Hinderer and H. Legros, in *Structure and Dynamics of Earth's Deep Interior*, D. E. Smylie and R. Hide, Eds. (AGU Geophys. Monogr. 46, 1988), pp. 79–82.
8. F. Roosbeek, *Geophys. J. Int.* **126**, 197 (1996).
9. D. E. Loper, *Phys. Earth Planet. Inter.* **11**, 43 (1975).
10. G. Williams, *Earth Planet. Sci. Lett.* **128**, 155 (1994).
11. K. Lambeck, *The Earth's Variable Rotation* (Cambridge Univ. Press, Cambridge, 1980).
12. M. N. Ross and G. Schubert, *J. Geophys. Res.* **94**, 9533 (1989).
13. S. Labrosse, J. P. Poirier, J. L. Le Mouel, *Phys. Earth Planet. Inter.* **99**, 1 (1997).
14. To compute the tidal potential in the past, we have taken into account the temporal evolution of the lunar-solar frequency (using the Kepler law and the Lagrange equations) and of the amplitude of the lunar potential (which varies as $1/d^3$, where d is the Earth-moon distance). An estimation of the temporal evolution of the removal of the moon is obtained from the conservation of the angular momentum of the Earth-moon system restricted to the axial rotation of Earth and to the orbital revolution of the moon.
15. J. P. Poirier, *Geophys. J. Int.* **92**, 99 (1988).
16. The change in the behavior of the dynamo precedes the surface events by a lag time equal to the sum of the length of time it takes the plume to erupt from the D″ layer after the resonance (that is, the characteristic time of the D″ layer responses to a thermal signal from the core) plus the length of time it takes the plume to rise to the surface.
17. K. C. Condie, *Palaeogeogr. Palaeoclimatol. Palaeoecol.* **75**, 57 (1989).
18. S. R. Taylor and S. M. McLennan, *The Continental Crust: Its Composition and Evolution* (Blackwell, Oxford, 1985).
19. J. G. Ogg, *Global Earth Physics, A Handbook of Physical Constants* (AGU Reference Shelf 1, T. J. Ahrens, Ed., 1995), pp. 240–265.
20. We thank S. Gilder for discussions and remarks on the original manuscript.

Eight Centuries of North Atlantic Ocean Atmosphere Variability

**David E. Black,[1]* Larry C. Peterson,[1] Jonathan T. Overpeck,[2]†
Alexey Kaplan,[3] Michael N. Evans,[3] Michaele Kashgarian[4]**

Climate in the tropical North Atlantic is controlled largely by variations in the strength of the trade winds, the position of the Intertropical Convergence Zone, and sea surface temperatures. A high-resolution study of Caribbean sediments provides a subdecadally resolved record of tropical upwelling and trade wind variability spanning the past 825 years. These results confirm the importance of a decadal (12- to 13-year) mode of Atlantic variability believed to be driven by coupled tropical ocean-atmosphere dynamics. Although a well-defined interdecadal mode of variability does not appear to be characteristic of the tropical Atlantic, there is evidence that century-scale variability is substantial. The tropical Atlantic may also have been involved in a major shift in Northern Hemisphere climate variability that took place about 700 years ago.

Although short-term variability in Atlantic climate is thought to be relatively well understood (1), both the patterns and the mechanisms of variability on decadal to century scales are as yet poorly known. In the southern Caribbean, the anoxic Cariaco Basin is well positioned to provide century- to millennium-length histories of trade wind–induced coastal upwelling (Fig. 1) as well as surface ocean changes that result from variations in the large-scale circulation of the Atlantic (2–4). Varved high-deposition-rate sediments [up to >100 cm per thousand years (ky)] and an abundance of microfossils result in one of the few marine records capable of preserving evidence of interannual- to century-scale climate variability in the tropical Atlantic. Between January and March, when the Intertropical Convergence Zone (ITCZ) moves close to the equator, strong easterly trade winds along the coast of Venezuela create intense Ekman upwelling and peak primary productivity over the Cariaco Basin and the continental margin (3, 5). Beginning in June or July, as the ITCZ moves north to a position near the Venezuelan coast, the trade winds diminish, and upwelling over the basin weakens. Studies of Cariaco Basin microplankton have shown that local populations dominated

[1]Rosenstiel School of Marine and Atmospheric Science, University of Miami, Miami, FL 33149, USA. [2]National Oceanic and Atmospheric Administration Paleoclimatology Program and the Institute for Arctic and Alpine Research, University of Colorado, Boulder, CO 80309, USA. [3]Lamont-Doherty Earth Observatory, Columbia University, Palisades, NY 10964, USA. [4]Center for Accelerator Mass Spectrometry, Lawrence Livermore National Laboratory, Livermore, CA 94551, USA.

*Present address: Department of Geological Sciences, University of South Carolina, Columbia, SC 29208, USA.
†Present address: Institute for the Study of Planet Earth, Department of Geosciences, University of Arizona, Tucson, AZ 85721, USA.

Fig. 1. Location and correlation map showing the spatial relation between variations in the abundance of the planktic foraminifer *G. bulloides* in the Cariaco Basin (southern Caribbean) and SST anomalies in the Atlantic Ocean. Mapped correlation coefficients (*r*) indicate the correlations between boxcar decadal-averaged *G. bulloides* data and historical SST anomaly data (*12*) for the time period 1856–1990 A.D. Correlations between *G. bulloides* abundance and SST anomaly time series are highest ($-0.8 < r < -0.9$, significant at the 99.9% level) in the North Atlantic region between 50° and 60°N, indicating that *G. bulloides* abundance, and hence trade wind–induced upwelling over the Cariaco Basin, are tightly coupled to SST anomalies in the northern North Atlantic region.
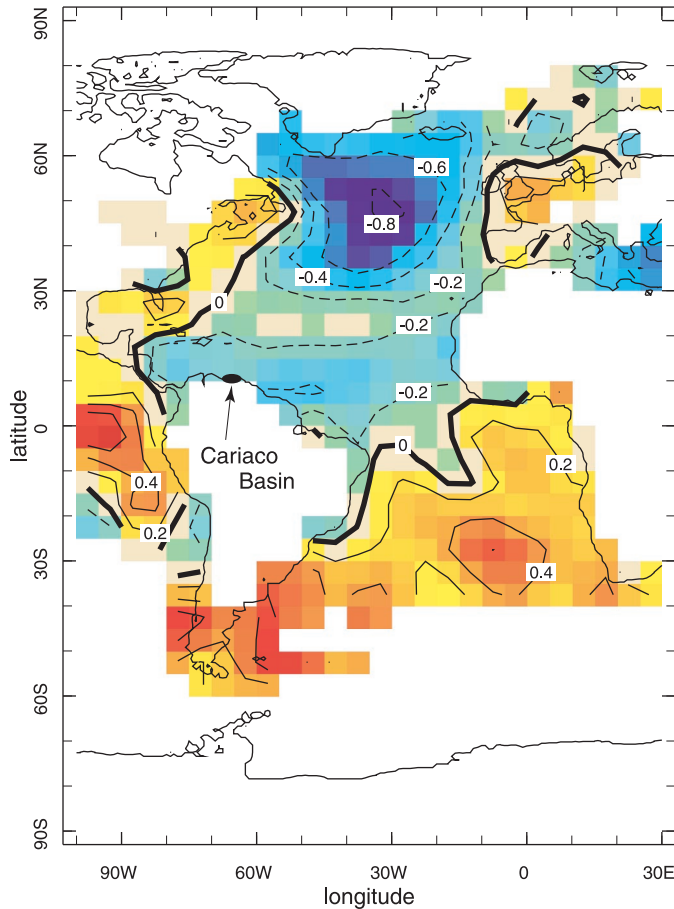
by the planktic foraminifer *Globigerina bulloides* reflect the cooler, more nutrient-rich waters found along the coast and that seasonal assemblage changes mirror the changes in upwelling intensity, and thus trade winds, over the year (*6*).

We sampled sediments from box core PL07-71 BC (395 m water depth), recovered from the gentle northern slope of the eastern Cariaco Basin, at continuous 1-mm intervals (*7*). The age model for core PL07–71 BC (Fig. 2) consists of two independently derived, mutually supporting age data sets. Age control for the upper 12.6 cm of the core (1880 to 1990 A.D.) is based on robust faunal correlations with a nearby box core already possessing a well-constrained ^{210}Pb and varve chronology (*8*). Below a depth of 12.6 cm, sediment laminations are less distinct and are difficult to count reliably. For this reason, below 12.6 cm (1165 to 1879 A.D.) the age model is based on a series of accelerator mass spectrometry (AMS) dates from monospecific samples of *G. bulloides*. Radiocarbon-based sedimentation rates for samples immediately at and below 12.7 cm are the same as the ^{210}Pb/varve-based estimates above 12.7 cm. The resulting 825-year record has a sample resolution of about one sample per year near the top of the record, decreasing to one sample per 2.5 years at the base.

The recent (1880 to 1990 A.D.) abundance record for *G. bulloides* illustrates sub-

Fig. 2. The age model for Cariaco Basin box core PL07-71 BC is based on a combination of ^{210}Pb, varve, and AMS ^{14}C chronologies. For the upper 12.6 cm of PL07-71 BC, the age model is based on detailed correlations to PL07-81 BC (**A**), a nearby box core that is already well dated by ^{210}Pb dating and varve counts (*8*), through an intermediate box core PL07-64 BC (**B**); dpm, disintegrations per minute. Cores PL07-81 BC and PL07-64 BC lie deeper in the basin and contain identical interbedded turbidites. Varve counts and ^{210}Pb values both indicate that the turbidites are not erosive and that a continuous sediment sequence is present in both cores. Sediments from PL07-64 BC (**B**) above and between the turbidites were sampled at continuous 1-mm intervals and analyzed for their planktic foraminiferal content. These data were used to develop faunal correlations between PL07-64 BC (**B**) and PL07-71 BC (**C**) and to transfer the established chronology from PL07-81 BC (**A**) to the latter. An example of this type of faunal correlation is shown for the foraminifer *Orbulina universa* (data shown as a three-point smooth); multiple taxa were used to check and verify the correlations. For sediment in core PL07-71 BC deposited at a depth between 12.6 and 56.4 cm (**D**), an interval where laminae were too faint to count, the age model is based on a series of 12 AMS ^{14}C dates measured on monospecific samples of *G. bulloides* (Table 1). Radiocarbon dates were converted to the calendar ages shown in (D) using a calibration model for marine samples (*35*); a local reservoir correction of 420 years, shown to be constant over periods of large climatic change, was used to account for radiocarbon differences between the surface waters and the atmosphere (*4*). Error bars represent the 1σ deviation; the unevenness of the error bars is a function of the marine calibration curve. A third-order regression line passing through both sets of age control points yields an r^2 of 0.98 and was used to assign calendar year ages to all samples in the box core deeper than 12.6 cm.
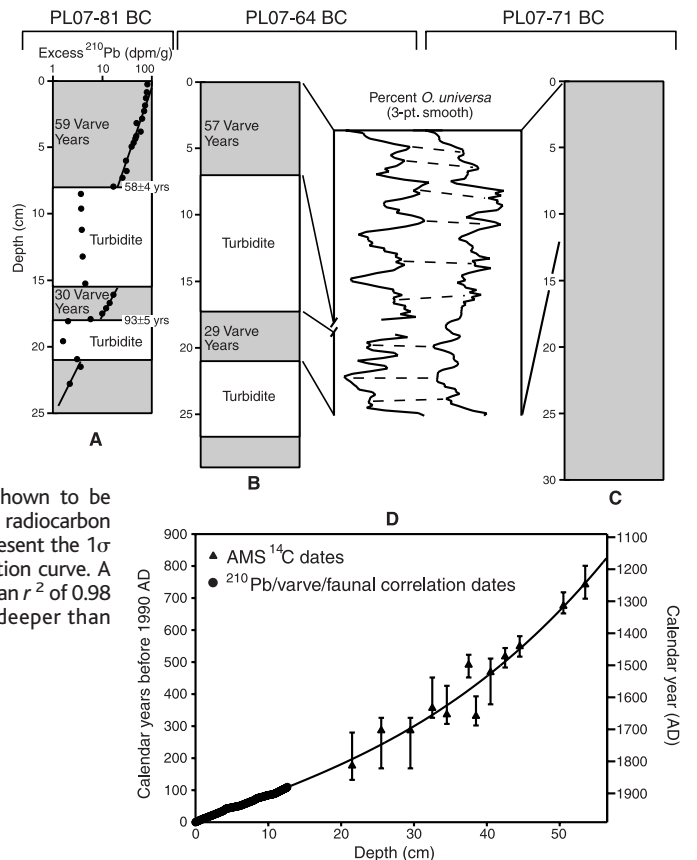
stantial variability that appears to be the result of changes in trade wind–induced upwelling intensity (Fig. 3A). Comparisons of *G. bulloides* abundance to a record of interhemispheric Atlantic sea surface temperature (SST) anomalies for the period 1901–1985 (Fig. 3B) (*9*) show that both records reflect well-known decadal-scale variations in tropical Atlantic surface conditions (*10*, *11*). Trade winds are more intense over the Cariaco Basin (as measured by increased *G. bulloides* abundance) when SSTs in the North Atlantic are colder than average, a pattern also seen when the *G. bulloides* data are compared directly to a record (*12*) of North Atlantic SST anomalies (45° to 65°N, 15° to 55°W; Fig. 3C). The overall relation between trade wind intensity and upwelling over the Cariaco Basin and Atlantic SSTs can be further illustrated in a spatial comparison of *G. bulloides* abundance to Atlantic SSTs (Fig. 1). Correlations are highest (significant at the 99.9% level) in the northern North Atlantic region between 50° to 60°N, confirming a robust association between intensification of the Atlantic trade winds and cold conditions in the northern North Atlantic region.

Previous work (*13*) indicates that when the cross-equatorial SST gradient in the Atlantic is reduced, the tropical North Atlantic is cool relative to the South Atlantic, resulting in increased surface pressure over the North Atlantic and a southward shift of the ITCZ. This leads to weakening of the southeasterly trades and intensification of the northeasterly trades, and hence to the stronger upwelling over the Cariaco Basin that is recorded by *G. bulloides* abundance. On decadal to interdecadal time scales, it has been suggested (*14*) that variability in the cross-equatorial SST gradient and wind intensity in the North Atlantic may be related to variability in Atlantic thermohaline circulation. Indeed, recent portions of the 1880–1990 A.D. *G. bulloides* abundance record correspond well to historical and instrumental evidence for North Atlantic circulation changes. During the 1970s, large negative salinity anomalies in the northern North Atlantic [the "Great Salinity Anomaly" (*15*)] were associated with unusually cold SSTs and substantially reduced deep convection in the Greenland Sea (*16*), one of the principal source regions of North Atlantic Deep Water. An inferred weakening of Gulf Stream flow during the 1970s accompanied this change (*17*), which was a time of higher *G. bulloides* abundance and stronger trade winds over the Cariaco Basin (Fig. 3). In contrast, stronger Gulf Stream flow during the 1950s occurred during a period of warmer North Atlantic SSTs and reduced *G. bulloides* abundance and trade wind strength in the southern Caribbean. However, the apparent lack of a temporal delay between increased *G. bulloides* abundance and cold SST anomalies and between decreased *G. bulloides* abundance and warm SST anomalies

in the northern North Atlantic (Fig. 1) argues strongly for atmospherically driven Atlantic linkages rather than oceanic ones, particularly at interannual time scales. It may be that high-latitude oceanic processes provide the initial conditions that set the stage for low latitude–high latitude atmospheric linkages on interannual time scales. Alternatively, it is possible that North Atlantic SSTs and associated changes in trade wind–controlled upwelling within the Cariaco Basin are driven from the tropics and precondition the North Atlantic's thermohaline variability (*18*).

The complete 825-year record of *G. bulloides* abundance and upwelling in the Cariaco Basin (Fig. 4A) exhibits the same level of distinct decadal variability as seen in the record of the past 110 years. Assuming that the recent correlation between wind stress and *G. bulloides* abundance holds in the older record, the *G. bulloides* data suggest that abrupt, large-magnitude changes in the North Atlantic trade wind system have occurred over longer time scales as well. Relatively long periods of stronger trade wind–induced upwelling are recorded between the years 1165–1360 A.D., 1410–1590 A.D., and 1640–1880 A.D., punctuated by intervals of weaker winds and lower foraminiferal productivity events centered at approximately 1380, 1620, and 1890 A.D.

For the period before about 1900 A.D., few data exist on trade wind variability in the southern Caribbean. Nevertheless, for the period 1640–1880 A.D., there are hints that support our inference that North Atlantic trade winds were stronger and that the ITCZ was positioned further south on average. A southward shift of the ITCZ between 1600 and 1900 A.D. has been previously postulated, based on scattered historical South American precipitation records (*19*). Coral $\delta^{18}O$ data from the Gulf of Panama have also been interpreted to indicate an intensification and southward shift of the trade winds between 1650 and 1800 A.D. (*20*).

Independent pre–20th century climatological records from the North Atlantic with resolution comparable to that of the Cariaco Basin record are sparse, but they do support inferences based on the Cariaco Basin *G. bulloides* abundance patterns. Fluctuations in records of summer ice core melt from Svalbard and periods of increased sea ice around Iceland match intervals of increased *G. bulloides* abundance (*21*), which suggests that the recent relation between colder northern North Atlantic SSTs and increased *G. bulloides* in the Cariaco Basin was maintained for the earlier period. In contrast, the *G. bulloides* abundance record does not appear to correlate well with the three-millennia record of SSTs from the Bermuda

Fig. 3. (**A**) Comparison of *G. bulloides* abundance data (solid line; data are plotted with increasing values downward) from box core PL07-71 BC to Comprehensive Ocean-Atmosphere Data Set zonal wind speed data (dotted line) (*36*) for the grid square centered on the Cariaco Basin (11°N, 65°W). Wind speed and *G. bulloides* abundance data in this panel are presented as 3-year boxcar averages for the period 1880–1990 A.D. Higher abundances of the upwelling-sensitive *G. bulloides* are associated with stronger zonal (trade) winds ($r = 0.66$, significant above the 99.9% level). (**B**) Comparison of *G. bulloides* abundance data (solid line) from PL07-71 BC to interhemispheric SST anomalies (vertical bars) over the Atlantic basin calculated from (*9*) for the time period 1901–1985 A.D. High abundances of *G. bulloides* are interpreted as evidence of strong upwelling and intensified trade winds in the southern Caribbean. Negative temperature anomalies indicate a pattern in which the North Atlantic is cool relative to a warm South Atlantic, with variations in this index describing the well-known Atlantic thermal dipole (*10*, *11*). The *G. bulloides* abundance record from the Cariaco Basin shows a clear decadal-scale correlation to the interhemispheric SST anomalies, with high *G. bulloides* abundances (strong trade winds and upwelling) associated with cooler North Atlantic temperatures. (**C**) Comparison of *G. bulloides* abundance data (solid line) with an index of North Atlantic SST anomalies (dashed line) (*12*), here calculated for the region of the Atlantic from 45° to 65°N and 15° to 55°W.
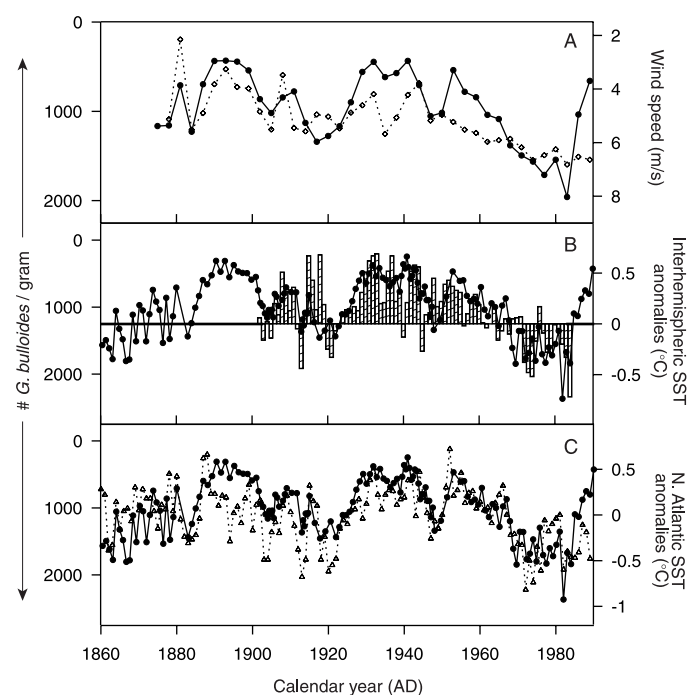
Table 1. Results of AMS radiocarbon dating of Cariaco Basin box core PL07-71 BC at the Center for AMS (CAMS), Lawrence Livermore National Laboratory. Meas., measured; cal., calender.

Depth (cm)	CAMS no.	Meas. age* (^{14}C yr B.P.)	Cal. age† (A.D.)	Cal. age range ±1σ (A.D.)
21.5	31642	530 ± 40	1814	1710–1858
25.5	31641	580 ± 60	1704	1664–1822
29.5	31640	580 ± 60	1704	1664–1822
32.0	31639	710 ± 50	1634	1538–1674
34.5	31638	680 ± 60	1654	1564–1683
37.5	31637	810 ± 50	1499	1467–1538
38.5	38292	670 ± 60	1659	1597–1688
40.5	31636	780 ± 60	1522	1479–1622
42.5	38293	850 ± 50	1473	1446–1507
44.5	31635	910 ± 60	1441	1409–1473
50.5	38294	1070 ± 50	1315	1272–1338
53.5	22810	1180 ± 60	1248	1189–1292

*Radiocarbon dates listed here have not been corrected for the 420-year age of the Cariaco Basin surface ocean reservoir.   †^{14}C ages were converted to calendar years according to (35).

Rise (22). However, correlations between Cariaco Basin *G. bulloides* abundance and SSTs in the region of the Bermuda Rise (northern Sargasso Sea; Fig. 1) are poor ($-0.2 < r < -0.4$) for the period since 1856 A.D., so there is probably little reason to expect a good correlation between the Cariaco Basin and Bermuda Rise records.

An important feature of the long-term *G. bulloides* record is a distinct change in the character of variability observed near the base of the record (Fig. 4). In sediments deposited before about 1320 A.D., *G. bulloides* abundance values fluctuate dramatically, with rapid high-amplitude changes of 300 to 400% occurring regularly in less than a decade. Since 1320 A.D., *G. bulloides* abundance values have varied more typically on the order of 100 to 200% on time scales of 10 to 20 years. This more modern-like variability regime came into being with the initial Little Ice Age cooling of the North Atlantic after 1300 A.D. (22, 23) and the demise of the Greenland Norse settlements (24). Other millennium-length records from the Northern Hemisphere show a change in the character of climate variability at approximately the same time. Tree ring–derived summer precipitation records from western North America show a change in character before 1400 A.D. at about the same time that extreme floods in the southwestern United States became more frequent (25). Lake sediment data from North Dakota also suggest a pronounced shift in drought regime around 1200 A.D., with droughts before this time characterized by greater magnitude, persistence, and frequency than droughts that have occurred since (26). A recent review of available data (27) supports the existence of a drought regime shift in western North America but notes that the timing may be somewhat later than 1200 A.D. and thus more in accord with the Cariaco Basin record. The implication is that regime shifts are a natural aspect of Atlantic variability and that these shifts may play a role in triggering changes in the frequency and persistence of drought over North America.

Spectral analysis of the *G. bulloides* time series was performed (28) to identify significant modes of Atlantic variability that might point to possible forcing mechanisms or related linkages (Fig. 4, inset). Results suggest that a century-scale mode of variability, distinct from the secular trend, appears to be an important natural aspect of Atlantic variability. Although the length of our new time series makes it is difficult to resolve the exact nature of this centennial mode, it is most likely related to long-term variations in the coupled ocean-atmosphere system, solar forcing, or a combination of these two. Climate model studies (29) indicate that significant interdecadal- to century-scale variability can result from processes (thermohaline circulation, for example) internal to Earth's climate system alone, but each model suggests a different time scale of dominant variability. The Cariaco Basin record indicates that the most important mode may be centennial rather than interdecadal in nature. This result contrasts with earlier analysis of the much shorter instrumental Atlantic record (30, 31), as well as of paleoclimatic data from land areas adjacent to the Atlantic (32), but it is quite plausible that an interdecadal mode is dominant in regions poorly correlated with Cariaco Basin variability (Fig. 1). Comparison of the *G. bulloides* record with one record of past solar variability (Fig. 4) (33) suggests that small changes in solar output may influence Atlantic variability on centennial time scales, a possibility supported by climate model experiments that indicate that solar variations can influence Hadley circulation and hence trade wind variability (34). Climate model results also suggest that past solar variability may have been large enough to affect the salinity balance of the North Atlantic and thus the thermohaline circulation, northward heat transport, and SST fields of the North Atlantic (34).

Over decadal time scales, the Cariaco Basin record demonstrates that significant spectral power in the 12.5- to 13-year band is an important long-term feature of natural Atlantic variability. In this case, the Cariaco Basin record confirms findings based on the instrumental record, where a nearly identical mode has been well documented (10, 30). This highlights the importance of tropical air-sea interactions in generating substantial decadal variability (10) and supports the hypothesis that Atlantic variability is linked to other tropical climatic variations [such as rainfall over the Sahel and northeast Brazil (9, 11, 13)] in a long-term fundamental way.

Fig. 4. Record of *G. bulloides* abundance variations (1-mm intervals) for the complete box core PL07-71 BC (from 0 to 56.4 cm), spanning the time interval from about 1165 to 1990 A.D. (solid line). Abundance data are plotted with increasing values upward. Given the increased perspective of the longer record, a strong pattern of interdecadal- to century-scale Atlantic variability is clearly seen to be superimposed on the decadal-scale variability of the past century. Spectral analysis (inset) (28) reveals concentrations of variance centered at periods of 140 to 500 years, 12.5 to 13.0 years, 8.7 to 9.0 years, 6.8 to 7.0 years, and 6.1 to 6.3 years (the Nyquist frequency is 1 cycle per 6 years; thus the inset has the entire spectrum). Also shown (main plot) is a visual comparison to calculated changes in ^{14}C production rate (dashed line) (33), which is one measure of changing solar activity in the past. Periods of reduced solar output (the well-known Maunder, Spörer, and Wolf Minima) correlate well with periods of high *G. bulloides* abundance in the Cariaco Basin (strong upwelling and trade winds), suggesting a possible role for solar forcing on these longer time scales.

References and Notes
1. S. Hastenrath, *Mon. Weather Rev.* **112**, 1097 (1984); R. G. Wagner, *J. Clim.* **9**, 2010 (1996).
2. J. T. Overpeck, L. C. Peterson, N. G. Kipp, D. Rind,

Nature **338**, 553 (1989); H.-L. Lin, L. C. Peterson, J. T. Overpeck, S. E. Trumbore, D. W. Murray, *Paleocean-ography* **12**, 415 (1997); G. H. Haug *et al.*, *Paleocean-ography* **13**, 427 (1998).

3. L. C. Peterson, J. T. Overpeck, N. G. Kipp, J. Imbrie, *Paleoceanography* **6**, 99 (1991).

4. K. A. Hughen, J. T. Overpeck, L. C. Peterson, S. Trum-bore, *Nature* **380** 51 (1996); K. A. Hughen *et al.*, *Nature* **391**, 65 (1998).

5. F. A. Richards, *Oceanogr. Mar. Biol. Annu. Rev.* **13**, 11 (1975); F. Muller-Karger and R. Aparicio-Castro, *Cont. Shelf Res.* **14**, 199 (1994).

6. M. D. de Miró, *Acta Geol. Hisp.* **6**, 102 (1971); K. A. Tedesco, R. C. Thunell, E. Tappa, F. Muller-Karger, R. Bohrer, *Eos* **78** (fall suppl.), F342 (1997).

7. Samples were washed through a 63-μm sieve and dried, and the >150-μm fractions were analyzed for their planktic foraminiferal content with a stan-dard binocular microscope. A total of 564 samples, each 1 mm thick, were used in this study. All data are archived at www.ngdc.noaa.gov/paleo/paleo.html.

8. K. A. Hughen, J. T. Overpeck, L. C. Peterson, R. F. Anderson, in *Palaeoclimatology and Palaeoceanogra-phy from Laminated Sediments*, A. E. S. Kemp, Ed. (Geological Society Spec. Publ. No. 116, The Geolog-ical Society, London, 1996), pp. 171–183; D. E. Black, thesis, Univ. of Miami, Coral Gables, FL (1998).

9. C. K. Folland, T. N. Palmer, D. E. Parker, *Nature* **320**, 602 (1986). Interhemispheric SST anomalies were recalculated as North Atlantic SST anomalies minus South Atlantic SST anomalies.

10. P. Chang, L. Ji, H. Li, *Nature* **385**, 516 (1997).

11. A. D. Moura and J. Shukla, *J. Atmos. Sci.* **38**, 2653 (1981); J. Servain, *J. Geophys. Res.* **96**, 15137 (1991).

12. A. Kaplan *et al.*, *J. Geophys. Res.* **103**, 18567 (1998).

13. S. Hastenrath and L. Greischar, *J. Geophys. Res.* **98**, 5093 (1993).

14. W. M. Gray, *Science* **249**, 1251 (1990); Y. Kushnir, *J. Clim.* **7**, 141 (1994).

15. R. R. Dickson, J. Meincke, S. A. Malmberg, A. J. Lee, *Prog. Oceanogr.* **20**, 103 (1988); S. Levitus, *J. Geo-phys. Res.* **94**, 9679 (1990).

16. P. Schlosser, G. Bönisch, M. Rhen, R. Bayer, *Science* **251**, 1054 (1991); L. A. Mysack and S. B. Power, *Climatol. Bull.* **25**, 81 (1991).

17. R. J. Greatbatch, A. F. Fanning, A. D. Goulding, S. Levitus, *J. Geophys. Res.* **96**, 22009 (1991).

18. A. W. Robertson, C. R. Mechoso, Y. -J. Kim, *J. Clim.*, in press.

19. W. A. Sanchez and J. E. Kutzbach, *Quat. Res.* **4**, 128 (1974).

20. P. W. Glynn, E. M. Druffel, R. B. Dunbar, *J. Mar. Res.* **41**, 605 (1983).

21. A. Tarussov, in *Climate Since A.D. 1500*, R. S. Bradley and P. D. Jones, Eds. (Routledge, London, 1992), pp. 505–516; L. Koch, *Meddeleser om Grønland* **130** (Copenhagen) (1945); A. E. J. Ogilvie, *Acta Archaeol.* **61**, 233 (1991); _____, in *Climate Since A.D. 1500*, R. S. Bradley and P. D. Jones, Eds. (Routledge, London, 1992), pp. 92–117.

22. L. D. Keigwin, *Science* **274**, 1504 (1996).

23. A. E. Jennings and N. J. Weiner, *Holocene* **6**, 179 (1996).

24. W. Dansgaard *et al.*, *Nature* **255**, 24 (1975); L. K. Barlow *et al.*, *Holocene* **7**, 489 (1997).

25. L. L. Ely, Y. Enzel, V. Baker, D. R. Cayan, *Science* **262**, 410 (1993); M. K. Hughes and J. J. Graumlich, in *Climatic Variations and Forcing Mechanisms of the Last 2000 Years*, P. D. Jones, R. S. Bradley, J. Jouzel, Eds. (Springer-Verlag, Berlin, 1996), pp. 109–124; H. D. Grissino-Mayer, in *Tree Rings, En-vironment, and Humanity*, J. S. Dean, D. M. Meko, T. W. Swetnam, Eds. (Radiocarbon, University of Arizona, 1996), pp. 191–204.

26. K. R. Laird, S. C. Fritz, K. A. Maasch, B. F. Cumming, *Nature* **384**, 552 (1996); K. R. Laird, S. C. Fritz, B. F. Cumming, *J. Paleolimnol.* **19**, 161 (1998).

27. C. A. Woodhouse and J. T. Overpeck, *Bull. Am. Me-teorol. Soc.* **79**, 2693 (1998).

28. The spectral analysis was done with the methods of M. E. Mann and J. M. Lees [*Clim. Change* **33**, 409 (1996)]. The power spectrum for the pre-1900 pre-industrial series was nearly identical to that of the complete record.

29. U. Mikolajewicz and E. Maier-Reimer, *Clim. Dyn.* **2**, 63 (1990); S. Manabe and R. J. Stouffer, *J. Clim.* **9**, 376 (1996); T. Delworth, S. Manabe, R. J. Stouffer, *Geo-phys. Res. Lett.* **24**, 257 (1997); A. Timmerman and M. Latif, *J. Clim.* **11**, 1906 (1998).

30. M. E. Mann and J. Park, *J. Geophys. Res.* **99**, 25,819 (1994); V. M. Mehta and T. Delworth, *J. Clim.* **8**, 172 (1995).

31. M. E. Schlesinger and N. Ramankutty, *Nature* **367**, 723 (1994).

32. M. E. Mann, J. Park, R. S. Bradley, *Nature* **378**, 266 (1995); M. E. Mann, R. S. Bradley, M. K. Hughes, *Nature* **392**, 779 (1998).

33. M. Stuiver and P. D. Quay, *Science* **207**, 11 (1980).

34. D. Rind and J. T. Overpeck, *Quat. Sci. Rev.* **12**, 357 (1993).

35. M. Stuiver and T. F. Braziunas, *Radiocarbon* **35**, 137 (1993).

36. S. D. Woodruff, R. J. Slutz, R. L. Jeanne, P. M. Steurer, *Bull. Am. Meteorol. Soc.* **68**, 1239 (1987).

van der Waals Interactions in the Cl + HD Reaction

Dimitris Skouteris,[1] David E. Manolopoulos,[1] Wensheng Bian,[2] Hans-Joachim Werner,[2] Lih-Huey Lai,[3] Kopin Liu[3]

The van der Waals forces in the entrance valley of the Cl + HD reaction are shown here to play a decisive role in the reaction's dynamics. Exact quantum mechanical calculations of reactive scattering on a potential energy surface without Cl–HD van der Waals forces predict that the HCl and DCl products will be produced almost equally, whereas the same calculations on a new ab initio potential energy surface with van der Waals forces show a strong preference for the production of DCl. This preference is also seen in crossed molecular beam experiments on the reaction. The study of chemical reaction dynamics has now advanced to the stage where even comparatively weak van der Waals inter-actions can no longer be neglected in calculations of the potential energy surfaces of chemical reactions.

The idea that the structure of the transition state of a chemical reaction determines the overall thermal rate coefficient is deeply in-grained in our understanding of chemical re-actions, and it forms the basis of a number of approximate (*1*) and exact (*2*) theories of chemical reaction rates. However, there is no indication from these theories that the more detailed dynamics of chemical reactions will not be sensitive to regions of the potential energy surface that are far removed from the transition state region, such as the shallow wells in the reactant and product valleys that are caused by van der Waals interactions. Here we show that the van der Waals forces in the entrance valley of the Cl + HD reac-tion do in fact have a substantial effect on the outcome of this reaction when the HD mol-ecule is rotationally unexcited. This result has some precedent in the context of ion-mole-cule reactions, the rates of which are often dominated by long-range electrostatic forces and can be highly sensitive to the initial rotational state of the reactant molecule (*3*). However, ion-molecule reactions often pro-ceed without activation barriers, whereas the Cl + HD reaction is a classic example of an activated chemical reaction (*4*). Furthermore, the van der Waals forces in the entrance valley of the Cl + HD reaction are consider-ably weaker than the long-range forces in ion-molecule reactions. For example, the depth of the Cl–HD van der Waals well is less than one-tenth the height of the reaction barrier on the Cl + HD potential energy surface (Fig. 1). The fact that such weak van der Waals forces can actually affect the out-come of the reaction is quite remarkable.

The kinetics of the Cl + H_2 reaction and its deuterium-substituted isotopomers have been studied for well over a century. The reaction played a central role in the development of transition state theory (*4*), is an important ele-mentary step in the mechanism of the Cl_2 + H_2 → 2HCl chain reaction (*5*), and has been used as a textbook example of the kinetic isotope effect (*6*). A number of electronic potential energy surfaces have been developed for the reaction over the years, the most recent being the G3 potential energy surface of Truhlar *et al.* (*7*). This surface has been shown in variational transition state theory (VTST) calculations (*7*) to give excellent overall agreement with exper-imental thermal rate coefficients (*8*) for the Cl + H_2 and Cl + D_2 reactions over a wide temperature range. Furthermore, detailed quasi-

[1]Physical and Theoretical Chemistry Laboratory, South Parks Road, Oxford OX1 3QZ, UK. [2]Institut für Theoretische Chemie, Universität Stuttgart, Pfaffen-waldring 55, D-75069 Stuttgart, Germany. [3]Institute of Atomic and Molecular Sciences, Academia Sinica, Post Office Box 23-166, Taipei, Taiwan 10764.